*Proc. Lunar Planet. Sci.*, 12B (1981), p. 1623–1639.
Printed in the United States of America

# Structural study of Cactus Crater

Joana Vizgirda and Thomas J. Ahrens

Seismological Laboratory, California Institute of Technology, Pasadena, California 91125

**Abstract**—The detailed structure of Cactus Crater, a 105 m diameter nuclear explosion crater formed in water-saturated carbonate rock of Eniwetok Atoll, is delineated using the high to low Mg calcite diagenetic transition as a stratigraphic tracer. Outside Cactus, this transition is observed as a discontinuous horizon which appears to be depressed, possibly as a result of the cratering event, near the crater. Beneath the crater, this transition occurs gradually over a $4.5 \pm 0.5$ m interval, leading to the following conclusions: material inside Cactus Crater underwent primarily *in situ* brecciation and mixing, the maximum depth of the excavation cavity is 20 m below sea level, and a fallback breccia lens, if it exists, has a maximum thickness of 1 m. A central uplift of $4.5 \pm 0.5$ m is inferred from the observation that the transition interval occurs at a 4 to 5 m greater depth at 1/2 crater radius than in the center. The excavation process, deduced from the Mg calcite transition as well as gamma well log data, involves high velocity injection of strongly shocked material to form the excavation cavity lining. The *in situ* brecciation and mixing appears to be a turbulent process, probably facilitated by fluidization of the carbonate rock. Based on the Mg calcite transition patterns beneath the crater floor, dynamic rebound is inferred as the modification mechanism for Cactus Crater. Using the Melosh Bingham model for dynamic rebound, a maximum strength of ~1 bar is inferred for the cratered carbonate medium. This strength value is representative of clays, such as those in which Snowball, a chemical explosion crater having dimensions and features similar to Cactus', was formed. Comparisons between Cactus and meteorite impact craters are also presented.

## INTRODUCTION

Because of their stratified nature, sedimentary rocks, acting as target media for impact or explosion craters, offer favorable circumstances for detailed crater structure investigations. Meteorite impact craters in sedimentary rocks display deformational features such as folded and faulted central peaks (e.g., Sierra Madera; Howard *et al.*, 1972), rim deformation and ring faults (e.g., Decaturville: Offield and Pohn, 1979), and fallback and autochthonous breccia lenses (e.g., Gosses Bluff and Meteor Crater; Milton *et al.*, 1972 and Shoemaker, 1963). Explosion craters in stratified targets, such as Snowball (Roddy, 1976), provide evidence of similar cratering produced features. Laboratory scale cratering experiments using colored, layered targets, (see e.g., Gault *et al.*, 1968) corroborate the observed large scale phenomena. However, sedimentary crater (especially meteorite crater) structural observations are often sketchy and do not permit comprehensive analyses of impact induced deformation. In particular, data on a variety of possible sedimentary lithologies (with saturation and stratification as additional variables) are needed in order to allow a numerical assessment, or, at least a qualitative synthesis of the effect of target properties on crater morphologies.

The purpose of this study is two-fold. First of all, an attempt is made to present an accurate, detailed description of an explosion crater in uncemented to partially cemented carbonate sediments. As an addition to the available data base, such a description would aid in formulating a rigorous theoretical treatment of crater structural dependence on target characteristics. Secondly, detailed observations of the crater are used to infer cratering excavation and modification mechanisms, and these interpretations are then compared with theoretically and observationally based cratering models.

Cactus Crater, the object of this study, located on Runit Island in the North Pacific Eniwetok Atoll. It is one of the smallest of the Pacific Test Site nuclear craters. Insight into the details of Cactus Crater structure is provided by a unique stratigraphic tracer, the

diagenetic transition boundary between high and low magnesium calcite (described in the next section). This stratigraphic marker, together with other geochemical data, also serves as the basis for interpretation of cratering mechanisms responsible for the formation of Cactus Crater.

## CARBONATE MINERALOGY—BACKGROUND

It has long been observed that organically precipitated carbonate skeletal material contains relatively high concentrations (up to 30 weight %) of $MgCO_3$ (see e.g., Silliman, 1846; Bøggild, 1930). Chave (1952) showed that this magnesium is present in the mineral calcite, and not dolomite, as previously believed. In that study, $MgCO_3$ concentrations, determined by chemical analyses, were compared with X-ray diffraction spectra of the same samples. The results, shown as the solid line in Fig. 1, indicate a continuous decrease in the (104) d spacing of the calcite lattice with increasing $MgCO_3$ content.

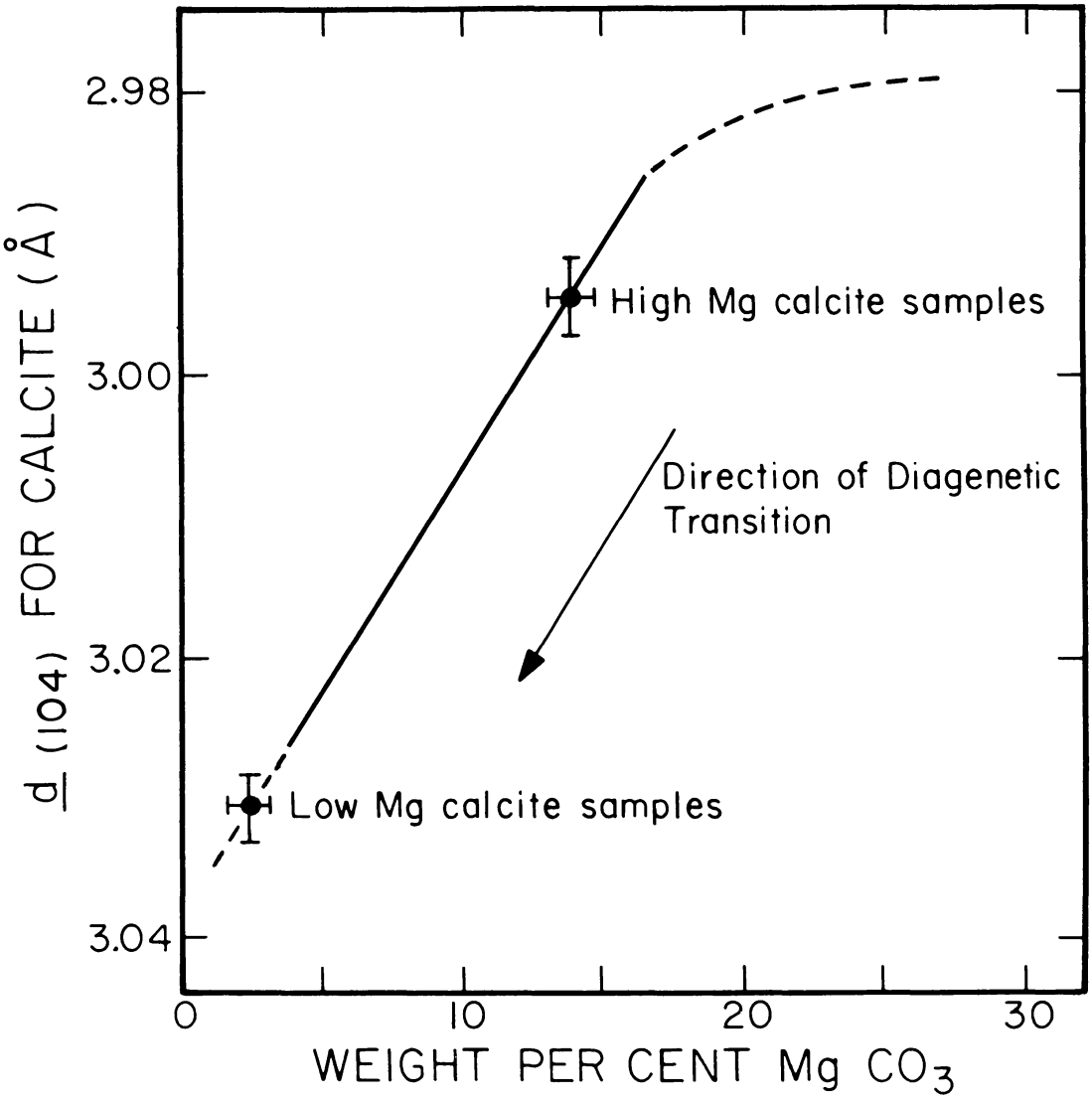


**Fig. 1.** Curve relating chemically determined weight % $MgCO_3$ and the (104) d spacing calculated from powder X-ray diffractometer scans of magnesian calcites; dashed portions represent considerable data scatter. (From: Chave, 1952). Points representing the range of d spacings observed for the high and low Mg calcites in Runit core samples are indicated. These variations were translated to represent compositional variations.

However, the equilibrium composition at earth's surface conditions of inorganically precipitated calcite is approximately 1 weight % $MgCO_3$ (Plummer and Mackenzie, 1974). Organically precipitated calcite with $MgCO_3$ concentrations of up to 30 weight % is, therefore, unstable at near surface conditions (excluding, of course, the biological environment in which it was produced). Thus, it is inevitable that magnesian calcite will alter to a more stable form. The method of magnesian calcite stabilization for Eniwetok samples probably involves dissolution resulting in calcite precipitation (containing less than 4 weight % $MgCO_3$) and a magnesium enriched solution, according to the following reaction (Land, 1967):

$$(Ca_{1-x}Mg_x)CO_3(\text{calcite}) + xH^+(aq) \rightleftarrows (1-x)CaCO_3(\text{calcite}) + xMg^{++}(aq) + xHCO_3^-(aq). \quad (1)$$

During sea-level lowstands relative to the atoll, typically associated with episodes of major glaciation, coral atolls are subaerially exposed. Meteoric waters percolate through the exposed coralline limestone dissolving the magnesian calcite and reprecipitating calcite with low (<4 weight %) Mg contents. As sea level rises, coral reef growth and (high) magnesian calcite deposition resumes on top of the altered low Mg calcite rock. It has been generally assumed (H. Lowenstam, 1980, pers. comm.) that the magnesian calcite diagenetic transition boundary produced under such conditions is a sharp discontinuity. Ristvet *et al.* (1974) first reported the presence of this diagenetic boundary at approximately 10 m depths on Eniwetok Atoll. Results on the detailed nature of this transition, as observed on Runit Island, are discussed in the following section.

## OBSERVATIONS

A detailed examination of the calcite mineralogy of samples from five cores drilled outside Cactus Crater, XRU-1, 3, 4, 5 and 6, (see Fig. 2) was conducted using powder X-ray diffractometry. X-ray data was obtained with a Norelco diffractometer using Ni-filtered Cu K$\alpha$ radiation and slow scan speeds of 0.25° $2\theta$ per minute; a minimum of 3 scans per sample were taken. Silicon powder (N.B.S. certified 99.9% pure) was used as an internal standard.

The X-ray spectra indicate the presence of two distinct calcite compositions (Fig. 1). In samples from deeper (below 15 m) levels of these cores, the strongest calcite reflection [corresponding to the (104) plane] is observed to occur between 29.43° and 29.48° $2\theta$, corresponding to d spacings of 3.032 Å and 3.027 Å, respectively. According to the relation between weight % $MgCO_3$ and $d_{(104)}$ spacings (hence $2\theta$ values) determined by Chave (1952) and reproduced in Fig. 1, reflections in this range correspond to $MgCO_3$ concentrations of $2.3 \pm 0.8$ weight %. Judging from the considerable scatter in Chave's data at $MgCO_3$ contents less than 3%, the actual variability in $MgCO_3$ content may be somewhat larger than this; however, it almost certainly does not exceed 4 weight %. The (104) calcite reflection in samples from shallower core levels occurs between 29.81° and 29.83° $2\theta$, corresponding to $MgCO_3$ concentrations of 13.8 to 14.5 weight %. $MgCO_3$ calcite contents intermediate between $2.3 \pm 0.8$ weight % and $14.15 \pm 0.35$ weight % (hereafter referred to as low and high Mg calcite) were not observed. As discussed in the section on carbonate mineralogy, many organisms metastably precipitate calcite with relatively high $MgCO_3$ concentrations, which, upon exposure to meteoric waters, transforms to calcite with low $MgCO_3$ contents. This phenomenon is clearly illustrated by the XRU core samples. The high Mg calcite in the Runit samples probably represents skeletal material of foraminifera and calcareous algae. These organisms have been identified in Runit core samples (Couch *et al.*, 1975), and the observed $MgCO_3$ concentrations in calcite correspond to those reported by Chave (1954) for skeletal material of tropical water foraminifera and calcareous algae.

The significant observation to be made in our Runit core X-ray diffraction studies is the nature of the high to low Mg calcite transition. There were no samples from any of the

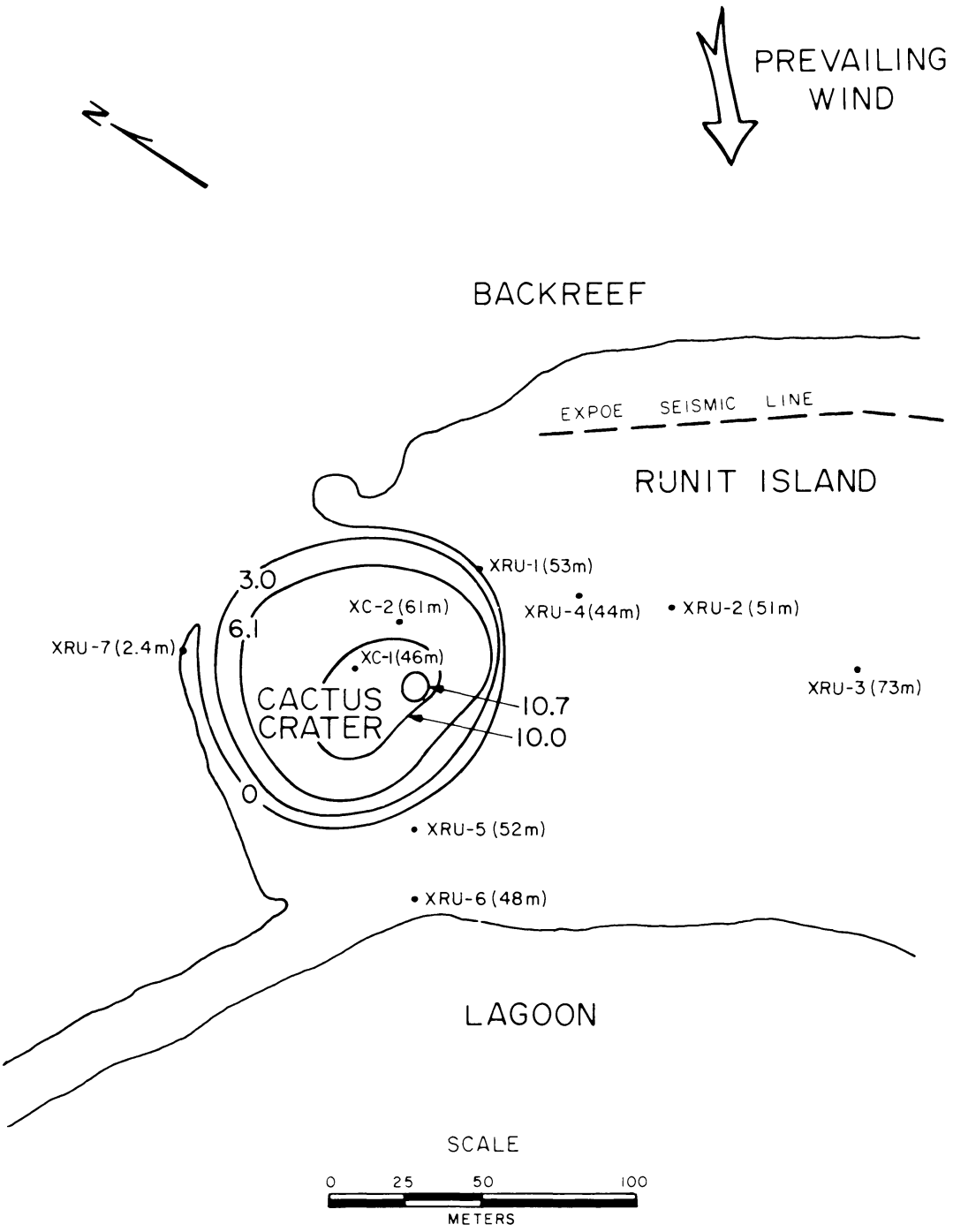


**Fig. 2.** Map of Runit Island, Eniwetok Atoll (11.30°N, 162.15°E) showing positions of drillholes in cratered (XC) and uncratered (XRU) portions of the island. Cactus Crater contour levels are difference contours. Dashed line indicates position of seismic refraction line.

XRU cores that contained both high and low Mg calcite. Therefore, within sampling interval limitations, magnesian calcite diagenesis on Runit Island (and, most likely, on all of Eniwetok Atoll) occurs as an abrupt transition. Depths to this transition in the XRU cores are listed in Table 1. All core sample depths are relative to the mean low water datum (Ristvet, 1981 pers. comm.). Differences in these depth levels may be a result of transectionally varying hydrologic regimes, or, may represent permanent, explosion induced displacements beneath Cactus Crater; these possibilities will be discussed in the next section.

**Table 1.** Runit diagenetic transition depths

| Core | Depth to High-to-Low Mg[1] Calcite Transition (m) |
|---|---|
| XRU-1 | 13.7 ± 1.3 |
| XRU-3 | 11.1 ± 0.5 |
| XRU-4 | 13.6 ± 0.4 |
| XRU-5 | 12.1 ± 1.0 |
| XRU-6 | 13.4 ± 0.6 |

[1]Depths are relative to the mean low water spring datum.

The nature of the high to low Mg calcite transition, as observed in samples from the cores drilled inside Cactus Crater, XC-1 and XC-2 (see Fig. 2), markedly differs from that observed in the XRU cores taken outside the crater. Both high and low Mg calcite X-ray diffraction peaks were observed in several samples from shallow (above 20 m) levels in the XC-1 and XC-2 cores. X-ray powder diffraction spectra of the 5 shallowest available XC-1 samples are shown in Fig. 3. Peaks of both high Mg and low Mg calcite, at ~29.8° and ~29.5° 2$\theta$, respectively, are present in the uppermost four of these samples. That of high Mg calcite, most prominent at the shallowest level, gradually decreases in intensity, while that of low Mg calcite increases in intensity with increasing depth in the core. At 15.4 m, and all levels below that, only low Mg calcite is observed. X-ray spectra of XC-2 core samples, reproduced in Fig. 4, show a similar pattern of consistently decreasing high Mg calcite and increasing low Mg calcite peak intensities. Below 20 m depth in XC-2, only the low Mg calcite peak is present.

X-ray powder diffraction spectra of XC-1 and XC-2 samples containing both high and low Mg calcite were analyzed according to the method described in the next section. (See Table 2 for Gaussian curve fit parameters.) Computer drawn observed and calculated fits to calcite peaks for four of the XC-1 samples are shown in Fig. 5. High Mg calcite concentrations were determined from integrated peak intensity ratios and the empirical calibration curve described in the next section. In Fig. 6, these concentrations are plotted against depth of sample for both XC-1 and XC-2 core material. Two noteworthy features are evident in this graph: first, the progressive nature of the two curves, and consequently, of the high to low Mg calcite transition in the XC-1 and XC-2 cores, and, secondly, the 4 to 5 m downward displacement of the XC-2 transition curve from that of XC-1. The significance of these two features will be addressed in the discussion section.

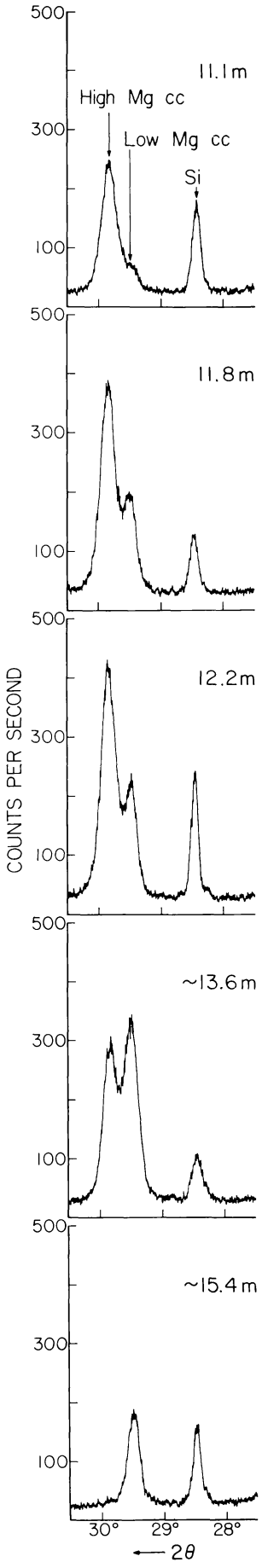


**Fig. 3.** Portions of powder X-ray diffractometer scans of the five shallowest XC-1 core samples. Sample depth levels are indicated in the upper right hand corner. Note the progressive variation in high and low Mg calcite (cc) peak intensities with depth in the core.

## QUANTITATIVE ANALYSIS

Relative concentrations of high and low Mg calcite can be determined from X-powder diffraction spectra. The analysis involves resolution of high and low Mg calcite component peaks, calculation of integrated peak intensities (i.e., peak areas), and comparison with an empirically derived composition vs. peak intensity curve. Although the specific technique differs, the analysis presented below is analogous to that used by Neumann (1965).

Component peak resolutions and integral peak intensities were obtained in the following manner. Sections of X-ray diffractometer spectra between 28.5° and 30.5° $2\theta$, totally encompassing the high and low Mg calcite peaks, were digitized; additional 1° $2\theta$ intervals on either side of these sections were used to determine a digitizing baseline. A least squares fit to the digitized data provided parameters A, B, C and D and their standard errors in the assumed Gaussian curve model:

$$I(\phi) = A \exp[-B^2(\phi - \omega)^2] + C \exp[-D^2(\phi - \omega - \Delta)^2] \quad (2)$$

where $I(\phi)$ is the peak intensity at some angle $\phi$ and $\Delta$ is the angular separation of the high and low Mg calcite peaks. $\omega$ is the centroid of the high Mg calcite peak:

$$\omega = \frac{\Sigma 2\theta I(2\theta)\Delta(2\theta)}{\Sigma I(2\theta)\Delta(2\theta)} \quad (3)$$

where $I(2\theta)$ is peak intensity at some angle $2\theta$ and $\Delta 2\theta$ is the angular increment. The high Mg calcite peak was sufficiently symmetrical so that its centroid coincided with the angle of maximum amplitude, 28.82° ± 0.01° $2\theta$. The angular separation was assumed constant at 0.37°. For the high Mg calcite peak, therefore, the integrated intensity is simply

$$\int_{-\infty}^{\infty} A \exp[-B^2(\phi - \omega)^2]\, d\phi = \sqrt{\pi}\frac{A}{B} \quad (4)$$

Similarly, the intensity of the low Mg calcite peak is $\sqrt{\pi}C/D$. Intensity errors are calculated from Gaussian parameter standard errors.

A calibration curve, relating weight % high Mg calcite to its fractional X-ray diffraction peak intensity, was constructed using samples of known high and low Mg calcite concentrations. The standard samples were prepared using XRU-3 core samples from 3 m (all high Mg calcite) and 58 m (all low Mg calcite) depths mixed in weight proportions of 1:9, 3:7, 5:5, 7:3 and 9:1. The weight % $MgCO_3$ was determined from this proportion and the weight % aragonite (determined

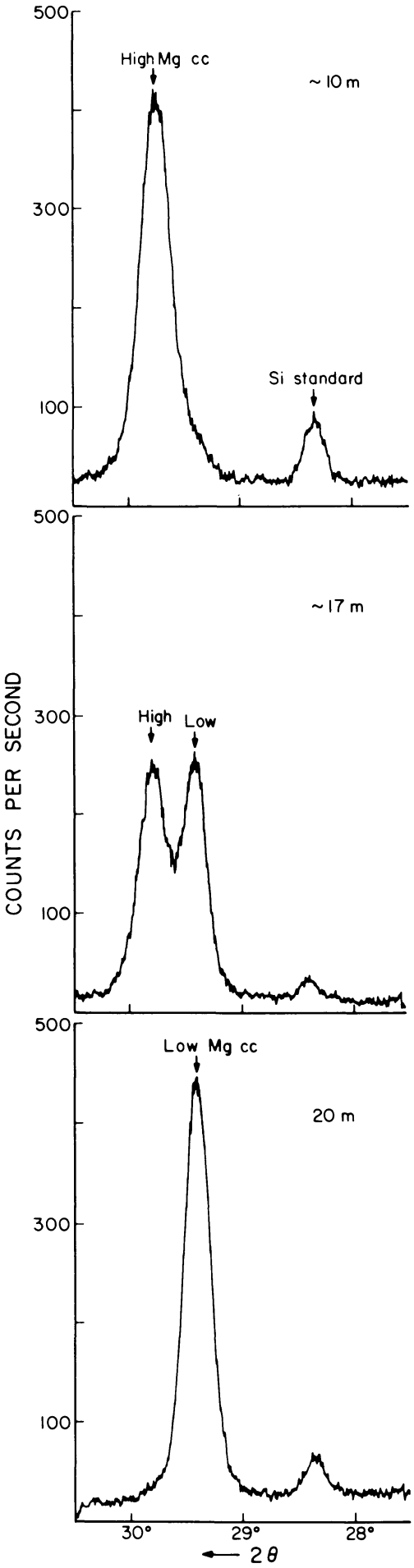


**Fig. 4.** Powder X-ray diffractometer spectra of XC-2 core samples. Note the progression from high to low Mg calcite with increasing depth in the core, and the similarity of this variation to that of XC-1 core samples, shown in Fig. 3.

using an X-ray calibration curve) in each sample. X-ray diffractometer spectra of these standard samples were then treated as described in the preceding paragraph and intensities of the high and low Mg calcite components were obtained. Gaussian curve fit parameters are listed in Table 2. Due to the extremely low intensity of the high Mg calcite peak in the 1:9 standard sample, a satisfactory fit to the data could not be obtained. At values of 25 weight % high Mg calcite and greater, the data lie on a straight line with a slope of 1/86.

## DISCUSSION OF CACTUS CRATER STRUCTURE

The role of the Cactus cratering event in explaining the observations presented above, and what these observations, together with other geologic and geophysical data can say about the process of crater formation, are discussed below.

An initial word of caution concerning sample depth levels is warranted. Due to coring difficulties and tidal variations during drilling, there is a 1.5 meter uncertainty in the location of XC-1 and XC-2 samples; this uncertainty is supplementary to the depth level error limits indicated in Fig. 6. (See Ristvet *et al.*, 1978, for elaboration on sampling uncertainties.) Although the arguments and conclusions presented below are not essentially altered by this additional uncertainty, quantitative values require critical assessment.

In order to evaluate possible cratering induced geologic changes, it is first necessary to establish what the undisturbed situation was. Specifically, information on the nature and positional variation of the high to low Mg calcite transition boundary is needed. As discussed in previous sections, the high to low Mg calcite transition is observed as an abrupt boundary in the XRU cores and occurs at depths between 11 and 14 m (see Table 1). Due to the role of meteoric diagenesis in this transition, a correlation between hydrologic regime and transition depth is expected. In subaerially exposed atolls such as Eniwetok, meteoric waters occur in a lens shaped configuration. It is thus anticipated that the depth to the high to low Mg calcite transition would vary along radial island transects but remain fairly

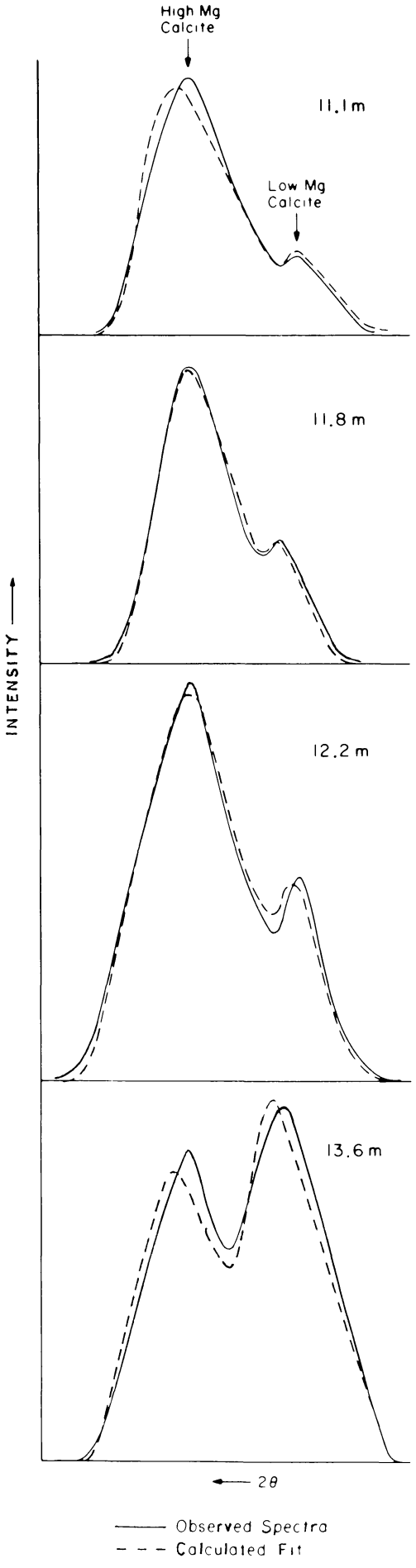


**Fig. 5.** Computer drawn observed and calculated X-ray diffraction peaks of high and low Mg calcite. Method used in calculating curve fits is described in the text.

**Table 2.** X-Ray peak Gaussian fit parameters

| | Sample | A | B | C | D[1] | $\frac{I_{High}}{I_{High}+I_{Low}}$[2] | Weight % High[3] Mg calcite |
|---|---|---|---|---|---|---|---|
| Calibration Samples | (High/Low Mg Calcite; weight %) | | | | | | |
| | 25/75 | 1.47 ± 0.12 | 3.37 ± 0.18 | 7.55 ± 0.06 | 2.92 ± 0.09 | 0.14 ± 0.03 | |
| | 44/56 | 3.67 ± 0.10 | 2.57 ± 0.15 | 7.65 ± 0.09 | 3.16 ± 0.11 | 0.37 ± 0.03 | |
| | 65/35 | 4.81 ± 0.10 | 2.46 ± 0.11 | 3.91 ± 0.09 | 3.30 ± 0.14 | 0.62 ± 0.03 | |
| | 88/12 | 6.20 ± 0.10 | 2.55 ± 0.15 | 1.58 ± 0.20 | 4.25 ± 0.21 | 0.87 ± 0.03 | |
| XC-1 Samples | (Depth; m) | | | | | | |
| | 11.1 | 3.95 ± 0.35 | 2.51 ± 0.55 | 0.48 ± 0.22 | 1.67 ± 0.61 | 0.85 ± 0.11 | 87 ± 10 |
| | 11.8 | 6.31 ± 0.18 | 2.44 ± 0.23 | 2.75 ± 0.20 | 3.65 ± 0.31 | 0.77 ± 0.05 | 80 ± 4 |
| | 12.2 | 4.44 ± 0.05 | 2.97 ± 0.13 | 1.78 ± 0.06 | 2.99 ± 0.12 | 0.72 ± 0.02 | 75 ± 2 |
| | 13.6 ± 0.9 | 4.82 ± 0.13 | 2.73 ± 0.22 | 5.86 ± 0.15 | 3.29 ± 0.27 | 0.50 ± 0.05 | 57 ± 4 |
| XC-2 Samples | (Depth; m) | | | | | | |
| | 15.2 ± 0.9 | 6.73 ± 0.38 | 2.26 ± 0.49 | 1.65 ± 0.44 | 5.34 ± 1.73 | 0.91 ± 0.07 | 93 ± 7 |
| | 17.2 ± 0.5 | 4.72 ± 0.27 | 2.00 ± 0.34 | 5.48 ± 0.17 | 3.71 ± 0.44 | 0.62 ± 0.08 | 68 ± 7 |

[1]Parameters A, B, C and D are related (but not numerically equal) to high Mg calcite peak height, width, low Mg calcite peak height and width, respectively. Gaussian fit model discussed in text.
[2]Integrated peak intensities of (high Mg calcite)/(high Mg calcite + low Mg calcite).
[3]Obtained comparing calculated intensity ratios with calibration curve.

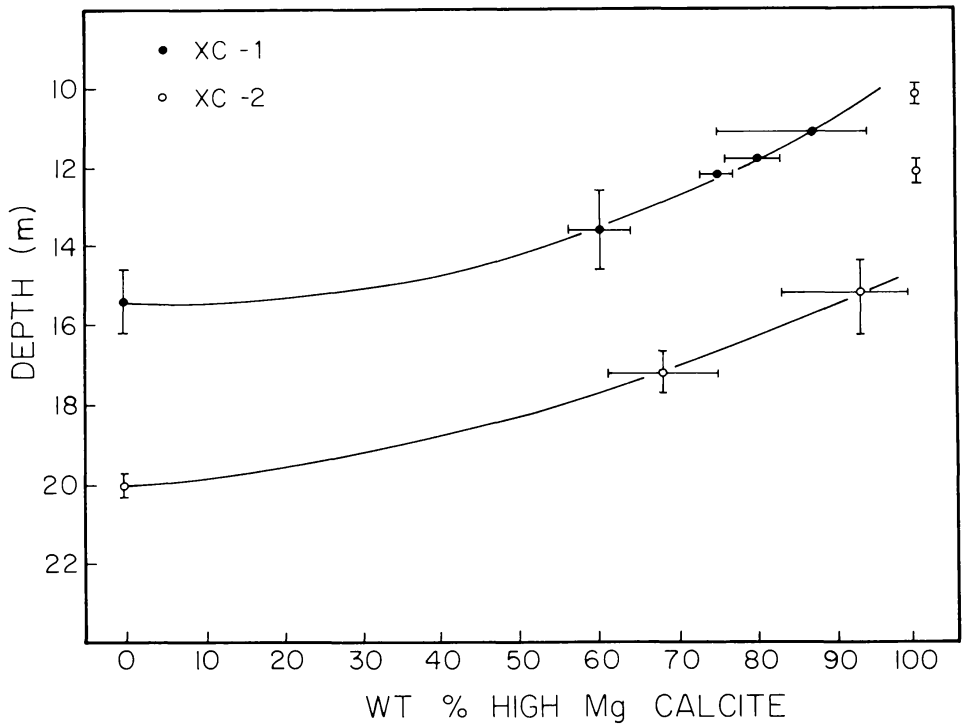


**Fig. 6.** Weight % high Mg calcite, as determined from powder X-ray diffraction spectra, vs. depth in the core. XC-1 and XC-2 samples are indicated by solid and open circles, respectively. Note the smooth variation in both cores of composition with depth and the 4 to 5 m displacement of the XC-2 from the XC-1 curve.

constant along any perimeter (i.e., circum-parallel to the reef crest). Ristvet *et al.* (1974) indicate that such lateral variations in diagenetic features of single stratigraphic units are observed at Eniwetok Atoll.

The Runit Island cores XRU-1, 4 and 3 were drilled in a line approximately parallel to both the elongated island outline and the reef crest. According to the argument just presented, depths to the high to low Mg calcite transition should be similar in these three cores. As noted in Table 1, however, the transition level in XRU-1 is depressed 1 to 3 m relative to that in XRU-3; a similar displacement is noted for XRU-4. These relations are illustrated in Fig. 7, a cross-section of Cactus Crater constructed from XRU and XC core data. The 20 and 35 m solution unconformities are based on Couch *et al.* (1975) data. The proximity of cores XRU-1 and 4 to Cactus Crater suggests possible cratering induced depression at these drill locations. Since the nature of the Mg calcite transition drastically changes directly beneath the crater, it is impossible to trace a sharp diagenetic transition into this area, and determining whether or not downward displacement is present here becomes difficult. Pressure attenuation considerations (Vizgirda and Ahrens, 1980) however, are consistent with stratigraphic depression occurring beneath the crater. According to results of this study, shock metamorphic levels in calcite from XC-1 require 4 to 5 m of downward displacement in order to accommodate theoretically reasonable pressure decay rates of d (depth)$^{-2}$ to d$^{-3}$. In addition, deeper solution unconformities (i.e., older than the first solution unconformity correlative with the Mg calcite transition) are observed to be depressed beneath the crater (see Fig. 7). Since no core samples below 2.5 m were obtained from locations to the north–west of the crater (i.e., in line with XRU-1 and XRU-3 but on the opposite side of the crater), the behavior of the solution unconformities across the crater cannot be determined. Nevertheless, available evidence from stratigraphic and pressure decay considerations suggest cratering induced depression beneath Cactus.

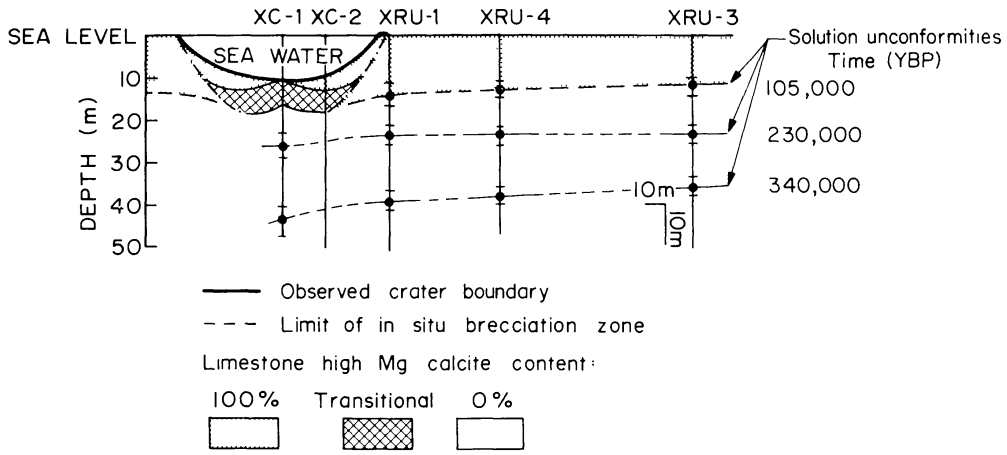


**Fig. 7.** Cross-section through Cactus Crater constructed on the basis of the high and low Mg calcite data and solution unconformity data of Couch *et al.* (1975). Note the apparent depression of the high to low Mg calcite transition boundary toward the cratered area and the inferred central peak inside the crater. The datum is mean low water level. (Two-fold vertical exaggeration.)

As discussed in previous sections, the nature of the high to low Mg calcite transition observed in samples from cores drilled inside Cactus Crater contrasts drastically with that observed in cores drilled outside the crater. The gradual change from all high to all low Mg calcite displayed by XC-1 and 2 core samples is not found anywhere else on Runit Island, nor is it expected considering the conditions under which the diagenesis occurs. Characteristics of this feature, unambiguously resulting from the cratering event, lead to several conclusions regarding the mechanics of crater formation.

First of all, the fact that the transition occurs in a consistent manner in both cores (see Figs. 2, 4 and 6), suggests that the material in this transitional interval was never ejected from the cavity, since ejection is not expected to result in such a finely stratified breccia lens. If a fallback breccia lens exists, it is limited at the center of the crater, i.e., at the XC-1 drill site, to a thickness of 1 m or less. This is the difference between the depths at which the hole was collared in and the first sample was retrieved. Instead, the bulk of material excavated during the cratering event experienced *in situ* brecciation and mixing. Mixing was probably initiated by material travelling radially downward and outward at particle velocities imparted after passage of the explosion-induced shock front. After brecciation of the originally saturated but competent coralline limestone, at least partial fluidization likely occurred, creating an inviscid, readily mixed substance. The turbulence of mixing was sufficient to completely homogenize hand specimen size samples. The extent of the gradational Mg calcite lens reflects the rate at which this turbulent mixing decreased with depth.

The observed pattern of the transitional Mg calcite layer also aids in the definition of the "excavation cavity". It the extrapolated "mixing lines" in Fig. 6 are valid, then the material experienced some degree of excavation, though not ejection, down to depths of approximately 15 and 20 m in XC-1 and XC-2 drill-core locations, respectively. Brecciation and mixing may have occurred at deeper levels within a totally low Mg calcite lithology, however, our methods would not allow its detection. The depths noted in previous sentences are, therefore, used to define the minimum limit of *in situ* brecciation sketched in Fig. 7.

Finally, the form of the transitional Mg calcite layer, sketched in Fig. 7 suggests a fundamental reclassification of Cactus Crater, which up to the present has been considered as belonging to the class of simple flat-floored craters. As depicted in Fig. 7, the transitional Mg calcite layer is 4 m thick in both cores and is depressed 4 to 5 m in XC-2 relative to that in XC-1. Neither of these observations is consistent with the structure of a

simple crater. Rather, the observation that the transitional layer occurs at shallower depths in the center of the crater than at a distance of one-half crater radius outward from the center is compatible with the interpretation of Cactus as a complex crater with a central uplift. Two other possibilities, namely depth uncertainties and structural inhomogeneities, must first be investigated before any firm conclusions concerning crater structure can be drawn. As mentioned in the beginning of this section, sample depth levels in the Cactus Crater cores are not precisely known. Nevertheless, the margin of error is insufficient to alter the conclusion regarding the existence of a central uplift; its extent, however, may be under or overestimated by up to 3 m. A second situation that may produce the observed pattern is the presence of some inhomogeneity in the cratered vicinity. In this case, the depiction of the Cactus floor as symmetrical would be inaccurate, and the structural classification ambiguous. Inhomogeneities do exist in Runit Island. For example, Ristvet *et al.* (1978) describe a cable berm located south of borehole XC-1. Lacking good geologic controls, in particular borehole evidence in the western portion of the island, this second possibility cannot be conclusively eliminated. However, as we shall see in the next section, the observation of a complex morphology in a small crater would not be an isolated case.

Seismic investigations conducted on Runit Island during Project EXPOE (Ristvet *et al.*, 1978) are limited to an approximately 550 m long seismic refraction profile obtained along the northeastern ocean margin (see Fig. 2). Based on this profile and geophysical logs of XRU boreholes, four seismic layers are distinguished in the upper 60 m of Runit. Apparent seismic velocities of these layers consistently vary from 0.4 km/sec to 3.1 km/sec with increasing depth, reflecting greater degrees of cementation. The shallowest layer represents unconsolidated supratidal sediments and is of uniform thickness along the extent of the seismic profile. The second layer, consisting of weakly to uncemented carbonate sediments, appears to thicken toward Cactus, and the interface (at approximately 15 m depths) between this and the third layer of moderately cemented carbonate rock appears to be depressed 3 m in the proximity of the crater. As mentioned earlier, and as shown in Fig. 7, two solution unconformities, occurring between 20 and 50 m depth, appear to be depressed beneath Cactus Crater; the extent of downward displacement is 6 m and 4 m for the first and second of these unconformities, respectively. On the basis of this, and the seismic evidence, Ristvet *et al.* (1978) also suggest that depression did occur beneath Cactus Crater.

Seismic velocities determined in the refraction profile may be used to further investigate the phenomenon of cratering induced brecciation. The velocities recorded for the second layer, i.e., the layer of unconsolidated to weakly cemented carbonate sediments, are observed to decrease consistently from 2.4 km/sec to 2.0 km/sec as one approaches the cratered area. Since this large a variation is not expected in a line parallel to the reef margin, it is inferred (Ristvet *et al.*, 1978) that the velocity decrease results from shock-induced brecciation beneath the crater. The depth of this lower velocity layer at the end of the refraction line closest to the crater is about 20 m below sea level. This depth is consistent with the observed maximum excavation limit below Cactus Crater of 20 m below the datum. On the basis of the high to low Mg calcite transition evidence from cores XRU-1 and XRU-4, where the transition was observed as a sharp diagenetic break, the disturbance causing decreased velocities involves fracturing, but no mixing.

Paleontological evidence (Ristvet *et al.* 1978) supports speculations involving brecciation and mixing beneath the crater and the extent of the excavation cavity. Pink, unbleached shells of the encrusting foraminifera, *Homotrema rubrum*, which indicate an origin above the first unconformity, are observed in XC-1 and 2 cores down to depths of $16 \pm 1.5$ m below the datum. Outside Cactus, unbleached shells are found only above the first solution unconformity, correlative with the Mg calcite transition depths, listed in Table 1. This fossil evidence is unclear in that it is not noted whether bleached and unbleached foraminifera shells are observed together at any level above 16 m beneath the crater. Such an observation would be analogous to the co-existence of both high and low Mg calcite in Cactus Crater cores. Nevertheless, the *Homotrema rubrum* evidence

supports mixing occurring to depths of $16 \pm 1.5$ m and the delineation of a minimum excavation cavity based on the Mg calcite data.

Gamma logs were obtained for most of the EXPOE boreholes. As anticipated, high radiation levels were recorded at several depths in boreholes XC-1 and XC-2; these patterns are reproduced in Fig. 8. Note the two high intensity peaks observed in both boreholes. As an accuracy check on the gamma log, radiation levels (primarily due to $^{60}$Co, $^{102}$Rh, $^{125}$Sb and $^{155}$Eu) of 24 split spoon samples were measured at the McClellan Central Laboratory, McClellan Air Force Base; this data is also presented in Fig. 8. These laboratory measurements corroborate both peaks observed in gamma logs of XC-1, and the shallower peak of XC-2. Lack of samples from 18 to 20 m depths of XC-2 may explain why the second high intensity radiation peak was not observed. Depths of the three laboratory observed high intensity peaks are consistently 2 m deeper than the well log data.

The observed distribution of gamma radiation serves to further elucidate the cratering process. Because peak penetration depths of nuclear fission products and neutrons are on the order of 10 $\mu$ and 1 m, respectively (see e.g., Fleischer *et al.*, 1975; Burnett and Woolum, 1974), peak radiation levels are produced only in substrate materials in close proximity (within 1 m) to the nuclear device. The observed post-event radiation intensity pattern, therefore, is a result of cratering produced particle motions. The observed radiation pattern in Cactus Crater may be the result of the following sequence of events. Material exhibiting the highest measured radiation levels originated closest to the nuclear device. As the shock wave from the explosion propagated into the target, high particle velocities were induced in the same material. Some of this material travelled radially into the target and formed a lining to the excavation cavity. Other particles, engulfed by the rarefaction wave produced upon reflection of the shock wave from the free surface of the target, were ejected at high velocities from the growing crater cavity. Some of these particles fell back into the cavity and constitute a thin fallback breccia lens. It is proposed that the shallow and deep high radiation intensity peaks represent the fallback and high velocity injected material, respectively. Ristvet *et al.* (1978) also propose forceful injection to explain the deeper peak. This interpretation is consistent with the crater formation model derived on the basis of the Mg calcite transition data. In addition, the crater excavation limits based on the gamma well log evidence (16 m and 19 m for XC-1 and XC-2 cores, respectively) agree well with those determined from the same Mg calcite transition.

## COMPARISONS WITH OTHER CRATERS AND CONCLUSIONS

In an attempt to gain a broader perspective of Cactus Crater in relation to other impact and explosion craters, the best comparison (in terms of size and substrate similarities) to be made is between Cactus and Snowball craters. The latter, described by Roddy (1976), is an experimental explosion crater, formed at the Defense Research Establishment, Suffield (Alberta) site by the detonation of 500 tons of TNT in saturated, unconsolidated layered clays, silts and silty sands. Snowball has a diameter of 107 m and a maximum depth of 9 m compared to respective dimensions of 105 m and 10.7 m for Cactus Crater. As in Cactus, water infilling occurred after the crater formed. A thin breccia lens (1 to 2 m) is observed at Snowball, corresponding to that speculated for Cactus. Major differences between the Cactus and Snowball sites are in the strength properties of the media, one being a basically competent but saturated coral rock, the other, saturated and completely unconsolidated sediments. There is a small difference in the heights of burst (HOB) of the two explosions. The 500 ton TNT hemisphere producing Snowball was detonated at ground level, i.e., zero HOB, whereas the 18 kTon TNT equivalent Cactus device had an approximately 1 m HOB. The similarity in size between the two craters despite the much greater (by a factor of 36) yield of Cactus is due to the greater cratering efficiency of high explosive, relative to nuclear explosive, sources. According to the empirical correlation curves in Cooper (1977), the cratering efficiency (defined as crater

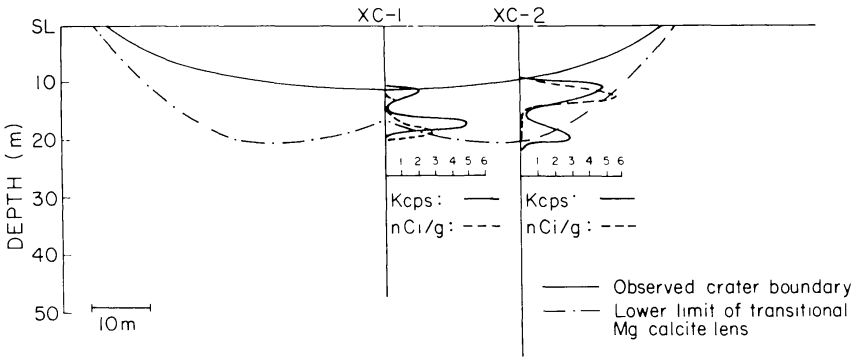


**Fig. 8.** Cactus Crater cross-section (no vertical exaggeration) showing gamma ($\gamma$) well log data (solid line) and laboratory measured total gamma activity (dashed line) for XC-1 and XC-2 cores; units for these two data sets are in kilocounts per second and nanocuries per gram, respectively. Figure is compiled from data presented in Ristvet *et al.*, 1978. (Datum is mean low water level.)

volume/yield) is 50 times greater for a high explosive relative to a high energy density nuclear explosive source for craters with HOB and volume characteristics of Snowball and Cactus. A distinct central peak structure, with an uplift of 8.5 m, is evident in Snowball. Although intensely folded, the clay and silt beds in this central mount retain sufficient integrity and can be mapped. Cactus, as speculated, also has a central peak, with 4 to 5 m of uplift. The rock making up this central structure, however, appears to be intensely shattered and mixed, and, had visually distinguishable units been present, they could probably not have been mapped. Thus, significant differences exist in the size and nature of the two central peaks. Furthermore, differences in the mode of disruption are observed away from the central peak. Numbered markers used in the Snowball experiment, allowing resolution of mass movements during cratering, indicate two discrete sets of motions occurred beneath the crater floor: the top layer moved radially outward, while material below it moved toward the center and up to form the central peak. Samples from the XC-2 Cactus core suggest turbulent brecciation and mixing compared to the (relatively) ordered movements beneath Snowball. It appears, therefore, that following shock-induced brecciation, the coral rock becomes less coherent than the silt and clay sediments. Differences in shock compression properties, or in the amount or distribution of water in the two types of substrates may be responsible for the varying behavior. Despite these differences, the two craters are similar in many respects, the most important being target saturation, and the analogy of Snowball to Cactus serves as an important feasibility argument for the description of Cactus as a complex crater.

Applying the Bingham plastic model of Melosh (1981) gives some indication of the material strength of the shocked coral material. According to this model, a minimum value of 5 for the dimensionless strength parameter, $\rho gH/c$, is required before crater collapse can occur; central peak formation requires a larger value, but the limiting case is considered here. Using a water-saturated coral density, $\rho$, of 2.4 g/cc (from measured bulk $\rho$) and a transient crater depth, H, of 20 m, a maximum Bingham yield stress of ~1 bar is calculated (g is the acceleration of gravity). Interestingly, yield stresses of the same order of magnitude have been measured for a variety of water-saturated clays, comparable to those at the Snowball Crater site (Wilson, 1927, p. 58–59). The yield stress, therefore, may be the critical parameter determining crater size and shape. There is potential then, according to this model, for quantitative treatment of crater structure target dependence.

Although information on terrestrial meteorite craters is often incomplete (or nonexistant), some comparisons between these craters and Cactus can be drawn. Where depth to the bottom of the breccia lens can be ascertained, the depth to diameter ratio of simple terrestrial craters is 1:3 (Dence *et al.*, 1977). Determining both the extent of the breccia lens and the rim position of the excavated cavity is particularly difficult for

complex structures, and the depth to diameter ratio of these craters is speculative. A palinspastic reconstruction of the Sierra Madera and Gosses Bluff structures suggests a ratio of 1:4 or 1:5 (Dence *et al.*, 1977). Using geologic observations and geophysical subsurface data, Pohl *et al.* (1977) speculate that the transient cavity of the Ries Crater had a similar depth to diameter ratio. The apparent 1:5 ratio for the true cavity of Cactus, therefore, is more compatible with that of complex structures.

Downward displacement has not actually been observed beneath any simple craters (Dence *et al.*, 1977), even those which offer sufficient stratigraphic control, such as Meteor Crater (Shoemaker, 1963). On the basis of attenuation rate arguments, however, Robertson and Grieve (1977) speculate that depression and approximately 50% shortening of the rock section beneath the crater occurred at Brent, a simple crater in crystalline rock. In complex craters, rocks in the ring surrounding the central peak typically appear to have undergone downward and inward motions. At the Red Wing Creek buried structure, there is some evidence, which eventually dies out at greater depth, for depression of rocks beneath the central peak (Brenan *et al.*, 1975). Stratigraphic depression beneath simple experimental impact craters has been clearly demonstrated by Gault *et al.* (1968), among others. In a laboratory scale study of explosive craters formed in loose saturated sand, Piekutowski (1977) observed downward displacement beneath a crater with a distinct central uplift. These laboratory studies, particularly those of Piekutowski which utilized saturated target materials, lend significant support to the speculated depression beneath Cactus.

In Vizgirda and Ahrens (1980), an attenuation rate of $(\text{depth})^{-5.7}$ is calculated for Cactus on the basis of electron spin resonance detected shock metamorphism; this rate is calculated in terms of post-flow stratigraphic coordinates. According to model calculations, downward displacement of 4 to 5 m is consistent with attenuation rates of $d^{-2}$ to $d^{-3}$. These rates are compatible with those inferred for simple craters (Robertson and Grieve, 1977). Considering the uncertainty in the estimate of displacement beneath Cactus, and the speculative nature of model attenuation rates, firm conclusions about either cannot be drawn. The interesting fact remains, however, that estimated amounts of displacement are consistent with reasonable attenuation rates.

The theorized thin (1 m or less) fallback breccia lens at Cactus is in agreement with general observations. Thin fallback breccia lenses, relative to the extent of autochthonous breccia, have been observed in both simple and complex structures, such as Meteor Crater (Shoemaker, 1963) and Gosses Bluff (Milton *et al.*, 1972).

The $\gamma$ ray intensity logs, discussed in the previous section, revealed two high intensity peaks, one located near the crater surface and the other at the hypothesized excavation cavity boundary. This pattern is similar to the distribution in melts or of intensely shocked and pulverized rock in simple craters in crystalline and sedimentary rock. At Brent and Lonar Lake Craters, formed in granitic gneiss and basalt, respectively, melt rocks are concentrated in the top and basal portions of the excavated cavity (Dence, 1968; Fredriksson *et al.*, 1973). At Meteor Crater, formed entirely in sedimentary rocks, meteorite fragments and highly shocked target rock are concentrated in similar positions (Shoemaker, 1963). These two layers of highly shocked material have not been clearly identified in complex craters. The extensive melt sheets described at complex craters, for example Manicouagan, are interpreted as the material lining the excavation cavity (Grieve and Floran, 1978). Melt layers are detected at two distinct intervals beneath the ring depression of Boltysh, a 20–25 km diameter structure in pre-Cambrian crystalline rock (Yurk *et al.*, 1975), however, the lower "unit" of melt was detected at only 1 borehole location and extended for a mere 20 m. Its lateral extent, thus, remains ambiguous, and a melt distribution analogy between Boltysh and simple craters cannot be justified. Based on the $\gamma$ log evidence, an analogy between Cactus and simple craters may be warranted.

Grieve *et al.* (1977), on the basis of impact melt distributions in simple and complex craters, proposed a common cratering model for both types of structures. Some of the interpretations stemming from Cactus Crater observations are consistent with their model. The inferred sequence of events and material motions during the Cactus excava-

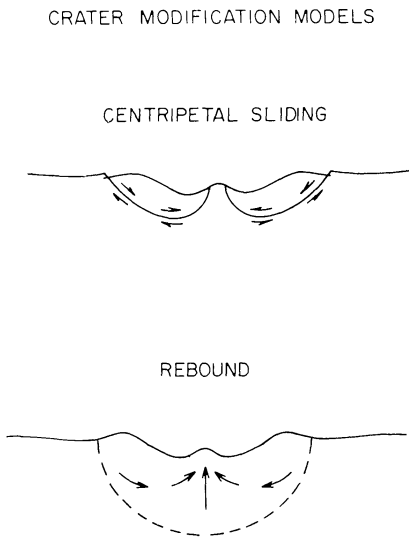


**Fig. 9.** Sketches depicting two possible crater modification mechanisms. Dashed line in the rebound model represents limit of region "fluidized" during excavation process (after Melosh, 1981). Reasons for preference of the rebound model for Cactus Crater are discussed in the text.

tion stage, for example, agree closely with that described by Grieve *et al.* Evidence for the modification mechanism acting at Cactus is less clear. Centripetal sliding (depicted in Fig. 9), a commonly invoked modification means for complex craters, produces an intensely disordered central peak. As evidenced in the orderly high to low Mg calcite transition in the XC-1 core, and its close similarity to the transition trend in XC-2, such disordering does not seem to have taken place in the central uplift of Cactus Crater. This observation suggests that a rebound mechanism (Fig. 9) rather than centripetal sliding may have produced the Cactus central peak. The Melosh (1981) Bingham plastic model assumes such a hydrodynamic rebound theory to explain various morphologic features of complex craters, such as central uplifts. If rebound, and not sliding, was indeed the active mechanism in the Cactus cratering event, then the observed crater diameter closely approximates that of the transient crater; the depth to diameter ratio of 1:5 would, thus be confirmed. The difference between this ratio and the 1:3 value commonly observed in simple craters suggests an essential difference in the transient crater geometry of simple and complex craters. This same suggestion has been proffered on the basis of terrestrial impact crater observations (see e.g., Pike, 1980) and experimental explosive crater investigations (Schmidt and Holsapple, 1981).

## SUMMARY

Summarizing the key observations and interpretations, Cactus Crater can be described as a 105 m diameter complex crater with 4 to 5 m of central uplift and possible downward displacement beneath the structure. Maximum depth of the excavation cavity is 20 m, and the resultant true crater depth to diameter ratio is 1:5. The majority of the breccia infilling the excavation cavity is of autochthonous origin and a fallback breccia lens, if it exists, is limited to a maximum thickness of 1 m. The excavation process, as deduced from Mg calcite and $\gamma$ log data, involves both ejection of some of the highly shocked material and high velocity injection of the remainder to form a lining to the transient crater floor. This *in situ* brecciation and mixing is envisioned as a very turbulent mechanism, facilitated by the high velocities and low viscosities of the intensely shocked and, probably, fluidized carbonate rock. Such a sequence of events is consistent with the crater excavation model of Grieve *et al.* (1977), deduced on the basis of impact melt distribution in terrestrial, particularly simple, craters. Thus, observations at Cactus Crater (specifically, the two peaks in the $\gamma$ log data, inferred to be analogous to the basal and upper melt layers in simple craters) serve to support a basic contention of the Grieve *et al.* model, that is, that a single excavation model can be applicable to both simple and complex craters. Cactus

Crater modification, on the basis of the Mg calcite study, is speculated to involve a dynamic rebound mechanism rather than centripetal sliding. Using the Bingham plastic rebound model of Melosh (1981), a maximum yield stress of ~1 bar is calculated for the shock-affected carbonate medium. Clays, such as those in which Snowball (an explosion crater with many features similar to Cactus) was formed, have comparable yield stresses.

Some of the features observed at Cactus have counterparts in terrestrial impact craters and may have been produced by the same processes. Application of a cratering model based on Cactus to other impact and explosion structures, however, should proceed with caution, since the unique properties of a water-saturated carbonate target may influence cratering mechanisms as well as modulate transitions between basic morphologic categories. The detailed observations presented here will, hopefully, contribute to the quantitative evaluation of target properties on crater morphologies, and serve as useful guidelines in the formulation of theoretical cratering models.

**Acknowledgments**—Discussions with B. Ristvet and J. Melosh are gratefully acknowledged. This research was supported under DNA contract 001-79-C-0252. Contribution No. 3615, Division of Geological and Planetary Sciences, California Institute of Technology, Pasadena, California 91125.

## REFERENCES

Bøggild O. B. (1930) The shell structure of the mollusks. *Danske Vidensk. Selsk. Skr.* **9**, pt. II, 235–326.

Brenan R. L., Peterson B. L., and Smith H. J. (1975) The origin of Red Wing Creek structure: McKenzie County, North Dakota, *Wyom. Geol. Assoc. Earth Sci. Bull.* **8**, 1–41.

Burnett D. S. and Woolum D. S. (1974) Lunar neutron capture as a tracer for regolith dynamics, *Proc. Lunar Sci. Conf. 5th*, p. 2061–2074.

Chave K. E. (1952) A solid solution between calcite and dolomite. *J. Geol.* **60**, 190–192.

Chave K. E. (1954) Aspects of the biogeochemistry of magnesium, calcareons marine organisms. *J. Geol.* **62**, 266–283.

Cooper H. F. Jr. (1977) A summary of explosion cratering phenomena relevant to meteor impact events. In *Impact and Explosion Cratering* (D. J. Roddy, R. O. Pepin, and R. B. Merrill, eds.), p. 11–44. Pergamon, N.Y.

Couch R. F., Fetzer J., Goter E., Ristvet B., Tremba E., Walter D., and Werdland V. (1975) Drilling Operations in Eniwetok Atoll During Project EXPOE. Air Force Weapons Laboratory, Rep. No. AFWL-TR-75-216. 267 pp.

Dence M. R. (1968) Shock zoning at Canadian craters: petrography and structural implications. In *Shock Metamorphism of Natural Materials* (B. M. French and N. M. Short, eds.), p. 169–184. Mono, Baltimore.

Dence M. R., Grieve R. A. F., and Robertson P. B. (1977) Terrestrial impact structures: principal characteristics and energy considerations. In *Impact and Explosion Cratering* (D. J. Roddy, R. O. Pepin, and R. B. Merrill, eds.), p. 247–275. Pergamon, N.Y.

Fleischer R. L., Price P. B., and Waler R. M. (1975) *Nuclear Tracks in Solids: Principles and Applications.* Univ. Calif., Berkeley. 605 pp.

Fredriksson K., Dube A., Milton D. J., and Balasundaram M. S. (1973) Lunar Lake, India: An impact crater in basalt. *Science* **180**, 862–864.

Gault D. E., Quaide W. L., and Oberbeck V. R. (1968) Impact cratering mechanics and structures. In *Shock Metamorphism of Natural Materials* (B. M. French and N. M. Short, eds.), p. 87–99. Mono, Baltimore.

Grieve R. A. F., Dence M. R., and Robertson P. B. (1977) Cratering processes: as interpreted from the occurrence of impact melts. In *Impact and Explosion Cratering* (D. J. Roddy, R. O. Pepin, and R. B. Merrill, eds.), p. 791–814. Pergamon, N.Y.

Grieve R. A. F. and Floran R. J. (1978) Manicouagan impact melt, Quebec Part 2. Chemical interrelations with basement and formational processes. *J. Geophys. Res.* **83**, 2761–2771.

Howard K. A., Offield T. W., and Wilshire H. G. (1972) Structure of Sierra Madera, Texas, as a guide to central peaks of lunar craters. *Geol. Soc. Amer. Bull.* **83**, 2795–2808.

Land L. S. (1967) Diagenesis of skeletal carbonates. *J. Sediment. Petrol.* **37**, 914–930.

Melosh H. J. (1981) A schematic model of crater modification by gravity. *J. Geophys. Res.* In press.

Milton D. J., Barlow B. C., Brett, R., Brown A. R., Glikson A. Y., Manwaring E. A., Moss F. J., Sedmik E. C. E., Van Son J., and Young G. A. (1972) Gosses Bluff impact structure, Australia. *Science* **175**, 1199–1207.

Neumann A. C. (1965) Processes of recent carbonate sedimentation in Harrington Sound, Bermuda. *Bull. Mar. Sci.* **15**, 987–1035.

Offield T. W. and Pohn H. A. (1979) Geology of the Decaturville impact structure, Missouri. *U.S. Geol. Survey. Prof. Paper* 1042. 48 pp.

Piekutowski A. J. (1977) Cratering mechanisms observed in laboratory-scale high-explosive experiments. In *Impact and Explosion Cratering* (D. J. Roddy, R. O. Pepin, and R. B. Merrill, eds.), p. 67–102. Pergamon, N.Y.

Pike R. J. (1980) Terrain dependence of crater morphology on Mars both yes and no (abstract). In *Lunar and Planetary Science XI*, p. 885–887. Lunar and Planetary Institute, Houston.

Plummer L. N. and Mackenzie F. T. (1974) Predicting mineral solubility from water data; application to the dissolution of magnesian calcites. *Amer. J. Sci.* **274**, 61–83.

Pohl J., Stöffler D., Gall H., and Ernstson K. (1977) The Ries impact crater. In *Impact and Explosion Cratering* (D. J. Roddy, R. O. Pepin, and R. B. Merrill, eds), p. 343–404. Pergamon, N.Y.

Ristvet B. L., Couch R. F., Fetzer J. D., Goter E. R., Tremba E. L., Walter D. R., and Wendland V. P. (1974) A Quaternary diagenetic history of Eniwetok Atoll (abstract). *Abstracts with Program, Geol. Soc. Amer.* **6**, 928–929.

Ristvet B. L., Tremba E. L., Couch R. F., Fetzer J. A., Goter E. R., Walter D. R., and Wendland V. P. (1978) Geologic and Geophysical Investigations of the Eniwetok Nuclear Craters. Air Force Weapons Laboratory, Rep. No. AFWL-TR-77-242. 330 pp.

Robertson P. B. and Grieve R. A. F. (1977) Shock attenuation at terrestrial impact structures. In *Impact and Explosion Cratering* (D. J. Roddy, R. O. Pepin, and R. B. Merrill, eds.), p. 687–702. Pergamon, N.Y.

Roddy D. J. (1976) High-explosive cratering analogs for bowl-shaped, central uplift, and multiring impact craters. *Proc. Lunar Sci. Conf. 7th*, p. 3027–3056.

Schmidt R. M. and Holsapple K. A. (1981) An experimental investigation of transient crater size (abstract). In *Lunar and Planetary Science XII*, p. 934–936. Lunar and Planetary Institute, Houston.

Shoemaker E. M. (1963) Impact mechanics at Meteor Crater, Arizona. In *The Moon, Meteorites and Comets* (D. M. Middlehurst and G. P. Kuiper, eds.), p. 301–336. Chicago, IL.

Silliman B. (1846) On the chemical composition of the calcareous corals. *Amer. J. Sci.* **1**, 2nd ser., p. 189–199.

Vizgirda J. and Ahrens T. J. (1980) Shock-induced effects in calcite from Cactus Crater. *Geochim. Cosmochim. Acta* **44**, 1059–1069.

Wilson H. (1978) *Ceramics Clay Technology.* McGraw-Hill, N.Y. 296 pp.

Yurk Y. Y., Yeremenko G. K., and Polkanov Y. A. (1975) The Boltysh depression—a fossil meteorite crater. *Int. Geol. Rev.* **18**, 196–202.